THE JOURNAL OF PHYSICAL CHEMISTRY A

Article

Cite This: J. Phys. Chem. A 2019, 123, 6160−6174

pubs.acs.org/JPCA

Nuclear Spin Symmetry Conservation Studied for Symmetric Top Molecules (CH_3D, CHD_3, CH_3F, and CH_3Cl) in Supersonic Jet Expansions

Published as part of The Journal of Physical Chemistry virtual special issue "Hanna Reisler Festschrift".

Veronika Horká-Zelenková,[†,‡] Georg Seyfang,[†] Peter Dietiker,[†] and Martin Quack*[,†]

[†]Laboratorium für Physikalische Chemie, ETH Zürich, Vladimir-Prelog-Weg 2, CH-8093 Zürich, Switzerland

[‡]J. Heyrovský Institute of Physical Chemistry of the CAS, Dolejskova 2155/3, 182 23 Prague 8, Czech Republic

ABSTRACT: We report results on nuclear spin symmetry conservation studied by high resolution spectroscopy of relative line intensities for the A and E nuclear spin isomers of symmetric top molecules CHD_3, CH_3D, CH_3F, and $CH_3{}^{35}Cl$ in supersonic jet expansions with He and Ar as carrier gases. Infrared absorption spectra were measured around 3000 cm^{-1} by an infrared (lead salt) diode laser and a continuous wave IR-OPO (infrared optical parametric oscillator) locked to a frequency comb. A detailed analysis of the R(2)-line intensities of the CH-stretching fundamental shows that nuclear spin symmetry is conserved for CHD_3, CH_3F, and $CH_3{}^{35}Cl$ during the expansion. For CH_3D, a small contribution from nuclear spin symmetry relaxation cannot be excluded completely under our experimental conditions.

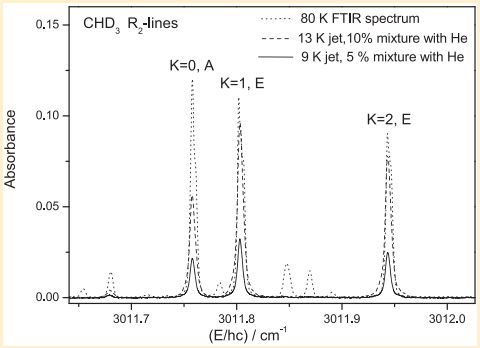

1. INTRODUCTION

Chemical reaction dynamics has many facets, to which notably Hanna Reisler has importantly contributed.[1−9] These include the state selective partitioning of energy among products in reactions of molecules and clusters. An important aspect which has found initial interest mostly with respect to the nature and energy of electronic states concerns symmetry in chemical reactions.[10−12] However, symmetry plays a much broader role in that different time scales of primary processes can be understood as arising from underlying approximate symmetries resulting in approximate constants of the motion being conserved in molecular processes and reactions.[13] One such approximate conservation law concerns nuclear spin symmetry, which results in detailed state to state selection rules in chemical reactions which have been predicted theoretically some time ago,[14] but for which only few experimental studies are available. Under certain circumstances, nuclear spin symmetry conservation even leads to the existence of fairly stable "chemical quasi-species".

Molecules possessing several identical nuclei with nonzero spin can exist in the form of different "nuclear spin isomers" corresponding to different nuclear spin symmetry species, which may have long lifetimes because of approximate nuclear spin symmetry conservation.[13] This resulted in the preparation of para-H_2 as a nuclear spin isomer already in 1929 through cooling in the presence of a magnetic catalyst.[15] Para-H_2 can be preserved for months without converting to ortho-H_2 at room temperature and even longer at reduced temperature and pressure. Nuclear spin symmetry conversion (relaxation) is a fundamental kinetic process, and so far, only few studies of such phenomena exist. We may mention in this context also early theoretical work.[16−18] Usually, however, nuclear spin symmetry conservation provides a strong selection rule in radiative transitions,[11,19−22] inelastic collisions,[21,23] and even chemical reactions.[14,24] Nuclear spin isomers play an important role in fundamental research of quite different fields such as astronomy and astrophysics in the study of the abundance of nuclear spin isomers in planetary and interstellar space, in the kinetics of chemical reactions in the gas phase, and in certain nuclear magnetic resonance (NMR) experiments.[25] A limitation in the study of nuclear spin isomers in the past was the development of a suitable separation technique, because the separation method used for ortho and para hydrogen is not suitable for heavy molecules, which have smaller rotational level splittings and a much higher boiling point. Therefore, the separation of nuclear spin isomers of heavy molecules requires special methods. Some separation techniques are summarized in a review by Chapovsky and Hermans,[26] and conversion between nuclear spin isomers can then be studied after separation. Alternatively, one can study the possible effects of nuclear spin symmetry interconversion by rapidly cooling a room temperature sample to very low temperatures for instance in supersonic jet expansions.[23,27,28]

Received: March 22, 2019
Revised: June 25, 2019
Published: July 15, 2019

DOI: 10.1021/acs.jpca.9b02580
J. Phys. Chem. A 2019, 123, 6160−6174

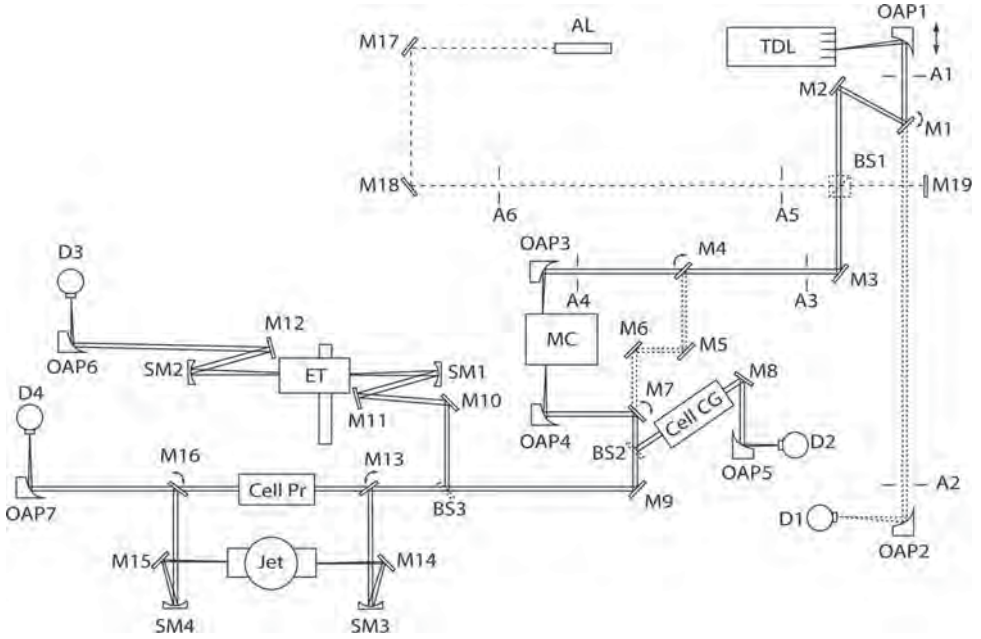

Figure 1. Block diagram of the diode laser spectrometer: A, aperture; AL, alignment laser; BS, beam splitter; Cell CG, cell with calibration gas; Cell Pr, cell with sample gas; D, detector; ET, etalon; Jet, molecular beam with slit nozzle; MC, monochromator; M, mirror (flipping mirrors are indicated with a direction indicator); OAP, off-axis parabolic mirror; SM, spherical mirror; TDL, diode laser.

The conversion or conservation of the nuclear spin symmetry has been a subject of interest over some decades, but only a small number of polyatomic molecules such as $^{12}CH_4$,[18,23,27,29−32] $^{13}CH_4$,[33] C_2H_4,[34,35] CH_3F,[36,37] $^{13}CH_3F$,[37] H_2CO,[18,38−40] and H_2O[41−51] have been studied. Nuclear spin modifications of ions and radicals were also under investigation.[24,52,53] Notably, the conservation of nuclear spin symmetry has been proven repeatedly for methane ($^{12}CH_4$ and $^{13}CH_4$) in supersonic jet expansions with Fourier transform infrared (FTIR) spectroscopy and diode laser spectroscopy.[23,27,29,31,33,54] There has been some recent debate about nuclear spin symmetry conservation in H_2O.[48,51] In a recent supersonic jet experiment with cavity ring-down laser spectroscopy, the conservation of nuclear spin symmetry was confirmed for low mole fractions of H_2O ($x_{H_2O} < 0.9\%$) in an Ar expansion.[45−47] However, for higher mole fractions of H_2O, and as a consequence, a higher rotational temperature nuclear spin relaxation was obtained from the intensities of the $2_{2,1} \leftarrow 1_{1,0}$, $2_{2,0} \leftarrow 1_{1,1}$, and $3_{2,1} \leftarrow 2_{1,2}$ transitions of the $2\nu_3$ vibrational transition around 7500 cm^{-1} (in the notation $J'_{K'_aK'_c} \leftarrow J''_{K''_aK''_c}$). The onset of nuclear spin symmetry relaxation with a higher mole fraction of H_2O was related to the formation of water clusters in the early stages of the supersonic jet expansion. In some of our previous work, we have also tried to study nuclear spin symmetry conservation in CF_4.[55] For this molecule, a rotational temperature well below 5 K would be necessary to detect the expected effects on the rotational line intensities from nuclear spin symmetry conservation, but at the experimentally accessible rotational temperatures such effects could not be tested significantly. Thus, methane $^{12,13}CH_4$ remains the only spherical top molecule, for which significant results are available. It would be of interest to have additional results for the symmetric top isotopomers of methane. In the current work we have extended our investigations to CH_3D, CHD_3 in a diode laser experiment with slit jet supersonic expansions and to CHD_3, CH_3F, and $CH_3{}^{35}Cl$ using also a continuous wave IR-OPO as a light source. In Section 2 we describe the experimental techniques. Section 3 describes the theoretical analysis of the data. Section 4 presents the experimental results, and in Section 5 we present the conclusions on the current status of the field in relation to other results. Some preliminary results from the present work were reported in ref 56.

2. EXPERIMENTAL SECTION

2.1. Experimental Setup. For the experiments, a combination of a supersonic jet expansion and a tunable lead salt diode laser (TDL) or a Nd:YAG-pumped continuous wave IR-OPO was used. The experimental setup for the TDL measurements is shown in Figure 1. A slit nozzle of 33 mm × 0.1 mm diameter was built using the design of our group at ETH Zürich[57] as modified but similar to an earlier design,[58] see also ref 28. The piston of the slit is periodically opened by a solenoid coil supplied with a home-built power supply. The repetition rate and opening time were limited by the efficiency of the pumping system. For the TDL measurements we used opening times of 300−500 μs and a repetition rate of approximately 1 Hz. For the pumping a combination of a rotary pump (Pfeiffer 2063C) with a pumping speed of 18 L/s and a turbomolecular pump (Pfeiffer TMH 1600C) with a pumping speed of 15'000 L/s (for nitrogen) was used. The TDL (Laser Analytics) was operating in the infrared spectral range around 2970−3060 cm^{-1}, and the diodes were mounted in a liquid nitrogen cooled laser head. As the laser diodes used did not show single mode behavior, it was necessary to use a monochromator for the separation of the laser modes. The beam of the TDL usually shows quite a strong divergence, depending on the type of laser and the laser parameters like laser temperature and current. The beam is made parallel with a combination of parabolic mirrors (OPA1) and directed through the monochromator (MC) to the detectors. Behind

DOI: 10.1021/acs.jpca.9b02580
J. Phys. Chem. A 2019, 123, 6160−6174

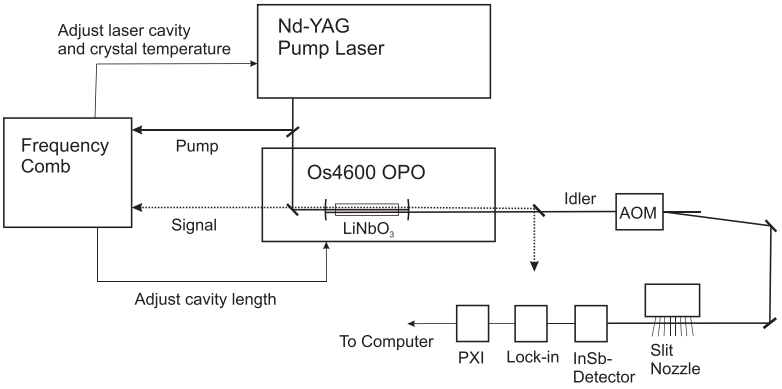

Figure 2. Experimental scheme to measure nuclear spin symmetry relaxation in a supersonic jet using a continuous wave IR-OPO locked to a frequency comb.

the monochromator the laser beam is split in three parts and guided through a cell filled with a reference gas (cell CG), with an etalon with a free spectral range of $\Delta\nu$ = 240 MHz used as a frequency marker, and then through the molecular beam chamber. The detector signals are collected by a multifunction data acquisition card (National Instruments, PXI 6225) with a sampling rate of 10 MHz for each channel and a vertical resolution of 12 bit. For every scan the data were transferred to the computer. The data acquisition card has 4 input channels (CH) which are detected in parallel (CH0, ramp of the diode current; CH1, signal from etalon (D3); CH2, signal from calibration cell (D2); CH3, signal from the jet (D4)). For the timing of the experiment a delay generator (Stanford, DG535) was used. For the triggering of the nozzle and for the adjustment of the pulse length of the molecular beam, a second identical pulse generator was used. During the opening time of the nozzle, a ramp was applied to the laser current to scan the laser across the desired spectral range. Depending on the scanning rate of the laser diode, a spectral range 0.5−1.0 cm^{-1} could be covered in a single scan. A background with the closed nozzle is measured separately in the TDL setup to obtain the absorbance (as ln I_0/I) of the measured spectra.

For a second set of experiments, a Nd:YAG-pumped continuous wave IR-OPO (Linos, OS4600) was used as a light source (Figure 2). As the OPO cannot be scanned through the desired spectral range within the time of one single molecular beam pulse, a stepwise acquisition scheme was employed. In this scheme the idler frequency of the OPO is tuned in small frequency steps where at every step the absorbance at the center of a number of molecular beam pulses was measured and averaged. To increase the sensitivity of the measurement, the idler radiation of the OPO was amplitude-modulated at 2 MHz with an acousto-optical modulator (IntraAction Corp., AGM-406A9M), sent through the jet chamber and detected by an InSb detector (Judson Inc., J10D). The detector signal was preamplified and sent to a lock-in amplifier (Stanford Research Systems, SR844) which was locked to the modulation frequency. The demodulated signal was then integrated with two boxcar-integrators (Stanford Research Systems, SR250). The gates of the integrators were set shortly before and at the central part of the jet pulse. The output of the two integrators was sent to a data acquisition card (National Instruments, PXI-6251) and used as background and signal, respectively, to calculate the absorbance. In order to remove the intensity fluctuations, the output of the lock-in amplifier was also sent through a low pass filter centered at 20 Hz and to a PI-controller (Stanford Research Systems, SIM960) which stabilizes the laser intensity by regulating the amplitude of the AOM-driving voltage. To ensure a linear frequency scan of the idler-beam, the pump and signal beams of the OPO were stabilized to different modes of a frequency comb (Menlo systems, FC1500-250). The idler frequency of the OPO is then calculated from

$$\nu_{\text{idler}} = (m_{\text{pump}} - m_{\text{signal}})\nu_{\text{rep}} + \nu_{\text{beat,pump}} - \nu_{\text{beat,signal}} \qquad (1)$$

where ν_{rep} is the repetition rate of the frequency comb, $\nu_{\text{beat,pump}}$ and $\nu_{\text{beat,signal}}$ are the offset beat frequencies of the pump and signal beams, and m_{pump} and m_{signal} are mode numbers of the frequency comb to which the signal and pump beams are locked. They are obtained sending the two laser beams to a wavemeter with a frequency precision better than half of the repetition rate of the frequency comb of 250 MHz. The idler frequency is scanned according to eq 1 through the variation of the comb repetition rate. The frequency accuracy of the idler radiation is determined by the external 10 MHz clock used as a reference for the frequency comb and can be estimated to better than 100 kHz.[59−61] A schematic view of the OPO setup is shown in Figure 2.

The effective resolution in the diode laser experiments is largely dominated by the averaging process for the different laser scans rather than the laser bandwidth of $\Delta\tilde{\nu}_{\text{L}}$ = 0.001 cm^{-1}. The effective resolution in the OPO experiment is much better, on the order of $\Delta\tilde{\nu}_{\text{OPO}} = 5 \times 10^{-5}$ cm^{-1}, and mostly determined by the stability of the locking of the OPO to the frequency comb.

2.2. Data Calibration in the Diode Laser Experiments and Samples. The data from the TDL-jet system have to be averaged over 50−150 scans. As during a scan only the variation of the signal is measured, the dc part of the signal has to be measured with a mechanical chopper. The absorbance is then calculated from the signal and background scans according to the Lambert−Beer law. The data are saved as a function of the ramp time t as $s_i(t)$. Even though the laser current is assumed to be linear with time, this is usually not true for the frequency of the light emitted by the diode laser, and therefore, the etalon fringes $s_n(n)$ are needed for a frequency calibration. For the small scan range ($\Delta\tilde{\nu} \leq 1.0$ cm^{-1}) of a single scan, it can be assumed that the frequency separation between the etalon fringes is constant. The positions of the etalon peaks are fitted as a function of time

DOI: 10.1021/acs.jpca.9b02580
J. Phys. Chem. A 2019, 123, 6160−6174

to a polynomial of order m. This allows the transformation of the measured spectra from a time scale $s_t(t)$ to a scale of etalon peak positions $s_n(n)$. The well-known line positions of the probed transitions in CH_3D and CD_3H are then used for the transformation of the signal from the n-scale of the etalon peaks $s_n(n)$ to the absolute frequency scale $s_{\tilde{\nu}}(\tilde{\nu})$. As the separation of the etalon peaks is not exactly known, we need at least two peak positions of the investigated sample within the scan range of the laser. The Fourier transform infrared spectroscopic measurements at 80 K used here for comparison as well were carried out in a special cooling cell setup described in ref 62 with our FTIR prototype spectrometer ZP2001 at essential Doppler limited resolution (see also refs 62 and 63).

The samples were commercially available: CHD_3 and CH_3D (98%, Cambridge Isotope Laboratories), CH_3F (Fluorochem, 99%), and CH_3Cl (Aldrich Chemicals, 99.5%). For the measurement of the infrared absorption spectra, mixtures with helium (Pangas, 99.96%) or argon (Pangas, 99.96%) as carrier gas were used. The mixtures were prepared with a mole fraction between $x_{sample} = 0.025$ and $x_{sample} = 0.1$ before the measurement in a stainless steel cylinder and then used in the supersonic jet expansion with backing pressures ranging from 0.5 to 3 bar.

3. THEORETICAL ANALYSIS OF THE DATA

3.1. Symmetry Considerations and Selection Rules.

The four molecules considered here all have C_{3v} point group symmetry, but for a more detailed understanding of the role of parity and nuclear spin symmetry it is useful to discuss the full permutation inversion group $S_3^* = S_3 \times S^*$ and its subgroup M_{S6}, which is the molecular symmetry group according to Longuet–Higgins.[64] We provide here a brief summary only, following also the notation in refs 13 and 14 which can be consulted for more detail. Table 1 gives the character table for

Table 1. Character Table for the Point Group C_{3v} and the Isomorphous Molecular Symmetry Group M_{S6} with the Induced Representation $\Gamma_m \uparrow S_3^*$[a]

C_{3v}	E	$2C_3$	$3\sigma_v$	
Class				
M_{S6} species	E	2(123)	3(12)*	$\Gamma_m \uparrow S_3^*$
A_1	1	1	1	$A_1^+ + A_2^-$
A_2	1	1	-1	$A_2^+ + A_1^-$
E	2	-1	0	$E^+ + E^-$

[a]After ref 14.

C_{3v} and the isomorphous group M_{S6} with symmetry species A_1, A_2, and E, which can be used to characterize the rovibrational levels. If one considers the possibility of inversion at the central carbon atom, one obtains a further tunnelling substructure of the levels which can then be classified in S_3^*. Because the barriers for inversion are very high,[65−68] the tunnelling substructure is nearly degenerate and each level in $C_{3v}(M_{S6})$ can be described as a nearly degenerate pair with symmetries according to the induced representation $\Gamma_m \uparrow S_3^*$, which is given in the last column of Table 1. The nuclear spin symmetry considerations for the sublevels are the same for the three molecules with the general formula CH_3X. The 2^3 nuclear spin functions for the three protons (Fermions) form a reducible representation $D_R = 4A_1^+ + 2E^+$, where the four A_1^+ functions correspond to the total nuclear spin $I(H_3) = 3/2$ (with $-3/2 \leq M_I \leq +3/2$) and the two E^+ functions to $I(H_3) = 1/2$ (with $M_I = \pm 1/2$). We write here the total nuclear spin multiplets as $^4A_1^+ + {}^2E^+$. The motional symmetry species Γ_m combine with the nuclear spin species Γ_{ns} to form the only Pauli-allowed species A_2^+ and A_2^-, i.e., $\Gamma_m \otimes \Gamma_{ns} = A_2^{\pm}$; therefore, the motional (rovibronic) wave functions of the A_2^+ and A_2^- species occur with nuclear spin species A_1^+ ($I = 3/2$), and the motional wave functions of species E^+ or E^- occur with the nuclear spin species E^+ ($I = 1/2$). The $A_1^{\pm}$ motional species have no Pauli-allowed partner among the nuclear spin functions and thus do not occur. This has also the consequence that for A_1 and A_2 levels in C_{3v} there is actually no tunnelling doublet, and each of these levels has a well-defined parity (label + or −), as A_1 in C_{3v} corresponds to a Pauli-allowed A_2^- level in S_3^* and A_2 in C_{3v} corresponds to A_2^+ in S_3^*. The E levels in C_{3v} have an allowed doublet structure with E^+ and E^- levels of different parity. As the sublevels of different parity are not resolved in general, the corresponding doublet is usually included in the "nuclear spin statistical weight", which has a contribution from the parity weight. For CHD_3 the 3^3 nuclear spin functions of the three deuterium nuclei generate a reducible representation corresponding in the multiplet notation to

$$[^7A_1^+(I = 3) + {}^3A_1^+(I = 1) + {}^1A_2^+(I = 0) + {}^5E^+(I = 2) + {}^3E^+(I = 1)]$$

These nuclear spin functions for the boson D^+ combine with the motional functions to Pauli-allowed overall total permutation symmetry species $A_1^{\pm}$. Thus, all levels in C_{3v} (A_1, A_2, E) result in tunnelling doublets of different parity ($A_1^{\pm}$, $A_2^{\pm}$, $E^{\pm}$) and a more complex D_3 - nuclear spin multiplet structure as given above. However, in our experiments none of the substructures are resolved, and one can distinguish for all four molecules only the nuclear spin symmetry "isomer" of A-type and E-type with the statistical weights arising from the multiplets as discussed and summarized in the simplified description given in the following section, keeping, however, the actual complexity in mind. The collisional selection rule is the conservation of nuclear spin symmetry (A or E), while the parity of one collision partner may change even if the total parity is assumed to be conserved. On the other hand the electric dipole selection rule is conservation of nuclear spin symmetry and change of parity in the molecule undergoing radiative one photon transitions, thus giving allowed electric dipole transitions in S_3^* as follows:

$$A_1^+ \leftrightarrow A_1^- \tag{2}$$

$$A_2^+ \leftrightarrow A_2^- \tag{3}$$

$$E^+ \leftrightarrow E^- \tag{4}$$

3.2. Energy Levels and Intensities.

We consider the vibrational ground state only for a symmetric top molecule at a given rotational temperature T_{rot}. The relative line intensity as integrated cross section[22,69,70] of a single rovibrational transition with the initial rotational quantum numbers J and K is given to within a good approximation by (with $G \simeq S/\tilde{\nu}_0$[69,70])

$$G_{JK} = \frac{1}{CL\tilde{\nu}_0}\int \ln(I_0/I)\, d\tilde{\nu} = aA_{KJ}N_K(2J + 1)g_I(\Gamma)\exp(-E_{KJ}/kT_{rot}) \tag{5}$$

DOI: 10.1021/acs.jpca.9b02580
J. Phys. Chem. A 2019, 123, 6160−6174

where L is the optical path length, C is the concentration as molecular particle density, and $\tilde{\nu}_0$ is the line center of the transition. Neglecting higher orders the term value of the vibrational ground state F_{KJ} is given by

$$F_{KJ} = E_{KJ}/hc = J(J+1)B_0 + (A_0 - B_0)K^2 \quad (6)$$

a is a constant independent of K and J and proportional to the absolute square of the electric dipole transition moment, N_K is the K-degeneracy which is 1 for $K = 0$ and 2 for $K \neq 0$, and A_0, B_0 are rotational constants of the vibrational ground state. The Hönl−London factors A_{KJ} are proportional to the absolute square of the rotational transition moment summed over all orientations of J. In the present case we consider a parallel band ($A_1 \rightarrow A_1$ transition) with $\Delta K = 0$, and the quantities A_{KJ} are

$$\text{for } \Delta J = +1 \quad A_{KJ} = \frac{(J+1)^2 - K^2}{(J+1)(2J+1)} \quad (7)$$

$$\text{for } \Delta J = 0 \quad A_{KJ} = \frac{K^2}{J(J+1)} \quad (8)$$

$$\text{for } \Delta J = -1 \quad A_{KJ} = \frac{J^2 - K^2}{J(2J+1)} \quad (9)$$

$g_I(\Gamma)$ is the nuclear spin statistical weight factor for the nuclear spin isomer Γ. For molecules with a 3-fold axis, as is the case for CH_3X (X = D, F, and Cl) and CHD_3, the ground state levels with $K = 0, 3, 6, 9...$ have A symmetry for the rotational subgroup and therefore a larger statistical weight than those with $K = 1, 2, 4, 5...$ belonging to the symmetry E. For the special case of three identical nuclei with spin I, the "nuclear spin statistical" weight factor g_I is given by eq 10 for K divisible by 3, including 0 (A rotational symmetry)

$$g_I(\Gamma) = \frac{1}{3}(2I+1)(4I^2 + 4I + 3) \quad (10)$$

and by eq 11 for K not divisible by 3 (E rotational symmetry)

$$g_I(\Gamma) = \frac{1}{3}(2I+1)(4I^2 + 4I) \quad (11)$$

For CH_3D and CHD_3 the lowest rotational levels are shown for illustration together with their rotational symmetry in Figure 3. Table 2 summarizes the rotational parameters used here for all molecules. If the different nuclear spin isomers are in thermal equilibrium, the rotational temperature T_{rot} is obtained from a plot of the logarithm of the line strength G_{JK} divided by the product of $(A_{KJ}N_K g_I)$ as a function of E_{KJ}/hc with the resulting slope $m = -hc/kT_{rot}$. Deviations from the equilibrium distribution for the different nuclear spin isomers can be obtained from measured line intensities. Following eq 5 the integrated cross section of a rotational line can be calculated from

$$G(J, K, \Gamma) = (\text{const})p(J, K, \Gamma)A_{KJ} \quad (12)$$

where Γ denotes the nuclear spin isomer A or E with a total nuclear spin of $I(H_3) = 1/2$ or $3/2$ for the three protons in CH_3X and $I(D_3) = 0$, 1, 2, or 3 for CHD_3.

After the expansion in a supersonic jet, the population of the states $p(J, K, \Gamma)$ can be considered for two extreme situations: with complete equilibration among all states (index r for relaxed distribution) or complete nuclear spin symmetry conservation (index c for conserved).[27] Assuming the same rotational temperature for all nuclear spin isomers, the relaxed distribution is given by

$$p_r(J, K, \Gamma) = g_I(\Gamma)N_K(2J+1)\exp[-E_{KJ}/kT_{rot}]/Q_r^{rot}(\text{tot}) \quad (13)$$

$Q_r^{rot}(\text{tot})$ is the relaxed rotational partition function including nuclear spin for a common rotational temperature T_{rot} and is calculated from

$$Q_r^{rot}(\text{tot}) = \sum_{\Gamma} Q_{rot}(\Gamma)\exp[-E_0(\Gamma)/kT_{rot}] \quad (14)$$

with

$$Q_{rot}(\Gamma) = \sum_J \sum_K g_I(\Gamma)N_K(2J+1)\exp[-(E_{KJ} - E_0(\Gamma))/kT_{rot}] \quad (15)$$

where $E_0(\Gamma)$ is the energy of the lowest level of the nuclear spin isomer Γ and E_{KJ} is energy for a given J and K in the vibrational ground state. For complete nuclear spin symmetry conservation one has

$$p_c(J, K, \Gamma, i) = x(\Gamma)N(\Gamma, J)(2J+1)\exp[-(E_{KJ} - E_0(\Gamma))/kT_{rot}]/Q_{rot}(\Gamma) \quad (16)$$

where $N(\Gamma, J)$ is the number of levels of isomer Γ for a given J and $x(\Gamma)$ is the mole fraction of the nuclear spin isomer Γ at the temperature T before the expansion, at which point the molecular spin isomers are assumed to be equilibrated. This mole fraction is given by

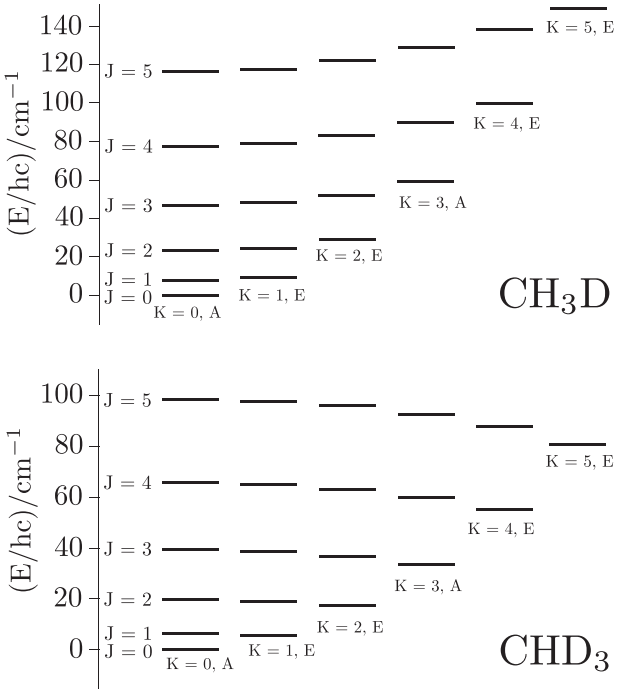

Figure 3. Level diagram for the vibrational ground state of CH_3D and CHD_3. The rotational energies are taken from ref 71 for CH_3D and from ref 77 for CHD_3 (see also refs 63 and 78 and references therein for more recent data, as well as refs 67, 79, and 80 for pure rotational spectra of CH_3D).

DOI: 10.1021/acs.jpca.9b02580
J. Phys. Chem. A 2019, 123, 6160−6174

Table 2. Ground State Rotational Constants of CH_3D, CHD_3, CH_3F, and $CH_3{}^{35}Cl$ Used To Calculate the Rotational Energy of the Probed Transitions[a]

	CH_3D	CHD_3	CH_3F	$CH_3{}^{35}Cl$
$A_0(C_0)/cm^{-1}$	5.2508208[71]	2.6289696[72]	5.182009[73]	5.205304[74]
B_0/cm^{-1}	3.8801946[71]	3.2791852[72]	0.85179425[73]	0.4434026[74]

[a]See also ref 63.

$$x(\Gamma) = Q_{rot}(\Gamma)\exp(-E_0(\Gamma)/kT)/Q_r^{rot}(tot) \quad (17)$$

The mole fraction of the nuclear spin isomers at high temperature follows from the regular density of the states and nuclear spin weights,[11,13,14,19,20,75,76] and $x(\Gamma)$ can be obtained from

$$x(\Gamma) \sim g_I(\Gamma)N(\Gamma) \quad (18)$$

where $N(\Gamma)$ is the high energy limit of the number of states of symmetry species Γ.

From eqs 10 and 11 one obtains the following for CHD_3: $x_c(A) = 11/27$ and $x_c(E) = 16/27$. One obtains the following for CH_3X: $x_c(A) = 1/2$ and $x_c(E) = 1/2$. For CHD_3, CH_3F, and CH_3Cl, the high temperature limit is reached already for a rotational temperature of 50 K, whereas for CH_3D small deviations from the high temperature limit are obtained ($x_A(50\ K) = 0.5006$, $x_E(50\ K) = 0.4994$). In the limiting case of $T_{rot} \rightarrow 0$ K only one single level ($J = K = 0$) is populated for complete nuclear spin symmetry relaxation whereas two levels (with $J'' = K'' = 0$ and $J'' = K'' = 1$ for CHD_3 or $J'' = 1$, $K'' = 0$ for CH_3D) are populated for nuclear spin symmetry conservation, and the ratio of the line intensities is given for molecules of the type CH_3X by the ratio of the corresponding Hönl–London factors.

The equations derived here for symmetric top molecules can also be extended to linear, asymmetric or spherical top molecules.[27,28,33,47]

4. RESULTS

4.1. General Aspects. The dynamics of collision induced nuclear spin symmetry relaxation in the expansion zone of a supersonic molecular beam was investigated for CH_3D and CHD_3 by diode laser absorption spectroscopy and for CH_3D, CH_3F, and CH_3Cl by scanning the IR-OPO across the absorption lines. If the nuclear spin isomer distribution is maintained during the expansion, then the nuclear spin isomers have to be considered as different chemical quasi-species. For each nuclear spin isomer, a separate distribution of the possible rotational levels is obtained after the expansion. As the isomers differ only in their nuclear spin symmetry, the assumption that the rotational distributions for the different nuclear spin isomers can be described by the same rotational temperature T_{rot} is usually justified. Each nuclear spin isomer will relax preferentially to its lowest rotational level as the temperature approaches 0 K.

To vary the rotational temperature in the molecular beam, several mixtures of the sample molecules with He were prepared and different backing pressures, ranging from 0.5 to 3 bar, were applied behind the slit nozzle. To investigate the dynamical processes during the expansion, the relative intensities of the measured absorption lines have to be determined with high accuracy. For the measurement with the diode laser this accuracy can only be achieved if all rotational lines considered are measured in a single scan, ensuring identical experimental conditions for all the lines. As the scanning range of the diode laser is 1 cm^{-1} at the most and as for molecules of the type CX_3Y the intensities of rotational lines with different K quantum numbers have to be compared, the experiments are preferentially done on the P- or R-branch of a parallel band ($A_1 \rightarrow A_1$ transition) with $\Delta K = 0$, because for a given quantum number J the lines for the different K quantum numbers are close enough to be covered in a single scan. Additional complications may arise from the fact that the complete spectral range is not reachable with a single laser diode.

The mode-hop free tuning range of the cw-OPO is limited by the pump laser to roughly 0.3 cm^{-1}. To cover the needed spectral range, it was therefore necessary to scan over several mode-hops which is not critical because of the referenced boxcar technique (details see above in the Experimental Section), where the absorbance is being obtained directly in the measurements.

Different criteria have to be considered for a proper choice of the measured rotational lines. Both nuclear spin isomers must have an absorption line in the considered spectral range, and at least one of the nuclear spin isomers must have more than one line to allow for the determination of a rotational temperature. All lines with $J = 2$ or larger fulfill these criteria. On the other hand, to decide whether the nuclear spin symmetry is conserved during the expansion phase of the molecular beam or not, rotational temperatures below 20 K have to be reached for the molecules investigated here (see below and Figures 7, 8, 11, and 15). For these temperatures, the rotational lines with $J = 3$ or larger are only weakly populated and the accuracy for the line intensities is less good. These two restrictions make the P(3)- or R(2)-lines of the symmetric CH-stretching fundamentals (ν_1) to be the ideal choice to study nuclear spin symmetry relaxation for CH_3X and CHD_3 in the expansion zone of a molecular beam. We use here the general notation ${}^{\Delta K}\Delta J_K(J)$ for the transitions, and because $\Delta K = 0$ also the simplified notation $\Delta J(J'', K'')$ or $\Delta J(J'')$ for several possible K'' (with symbol P for $\Delta K = K' - K'' = -1$ or $\Delta J = J' - J'' = -1$ and symbol Q for $\Delta K = 0$ or $\Delta J = 0$, or symbol R for $\Delta K = +1$ or $\Delta J = +1$), where by convention x'' is a quantum number of the lower level and x' the quantum number of the upper level in the transition.

To determine a reliable rotational temperature for all $J = 2$ lines from the measured molecular beam spectra the ratio of the line strength R(2, 1)-transition to the line strength of the R(2, 2)-transition has to be known as precisely as possible. According to eq 5 the rotational temperature is obtained from

$$T_{rot} = \frac{(E_{J=2,K=2} - E_{J=2,K=1})}{k \ln \frac{S_{J=2,K=1}A_{J=2,K=2}}{S_{J=2,K=2}A_{J=2,K=1}}} \quad (19)$$

where (with $J = J''$ and $K = K''$) E_i = rotational energy of the initial state i, S_i = measured line strength of the transition i, A_i = Hönl–London factor for the measured transition, and k = Boltzmann constant.

Differentiating T_{rot} with respect to the ratio of the line strengths one obtains:

DOI: 10.1021/acs.jpca.9b02580
J. Phys. Chem. A 2019, 123, 6160–6174

Table 3. Relative Line Intensities for T = 298 K for the R(2)-Lines of the ν_1 Fundamental for CH_3D Obtained from High Resolution FTIR Spectra and the Hitran Database[81] and Calculated According to Equation 5

J''	K''	J'	K'	Γ''_{rve}	$\tilde{\nu}_{0,FTIR}/cm^{-1}$	S^{rel}_{FTIR}	S^{rel}_{Hit}	S^{rel}_{cal}	$(S^{rel}_{Hit} - S^{rel}_{cal})/S^{rel}_{Hit}$
2	0	3	0	A	2993.35584(2)	0.4024	0.4121	0.4125	−0.00097
2	1	3	1	E	2993.25895(1)	0.3661	0.3606	0.3643	−0.01206
2	2	3	2	E	2992.91940(4)	0.2314	0.2272	0.2277	−0.0022

$$\frac{\delta T_{rot}}{T_{rot}} = \frac{S_{J=2,K=2}/S_{J=2,K=1}}{\ln(S_{J=2,K=1}A_{J=2,K=2})/(S_{J=2,K=2}A_{J=2,K=1})}\delta(S_{J=2,K=1}/S_{J=2,K=2}) \quad (20)$$

If we assume a rotational temperature T_{rot} = 20 K and an uncertainty of 5% for the ratio of the line strengths of the R(2, 1)- to the R(2, 2)-transition in CH_3D, we get an uncertainty of ΔT_{rot} = ±2.2 K for the rotational temperature determined from the molecular beam data. Considering the statistical uncertainty of our experimental results for the measured line intensities it is therefore necessary to know the relative line strengths with an uncertainty less than 3%. In Table 3 the relative line strengths obtained from our high resolution FTIR spectra at 298 K (normalized to 1.0) for the different R(2)-transitions of the ν_1 fundamental of CH_3D[63] are compared to theoretical values calculated from eq 5 and to relative line strengths obtained from the Hitran database.[81] The comparison shows that the uncertainty of the rotational temperature resulting from the reduced accuracy of the relative line strength is below 3 K for the rotational temperatures obtained in the molecular beam. The comparison between experimental and calculated values also shows that for these transitions the approximation for the intensities given by eq 5, neglecting higher order corrections such as Hermann−Wallis factors,[82] is adequate, as would be expected for these low quantum number transitions.

As the measured lines are weak, the accuracy of the experimental line intensities depends very crucially on a proper definition of the baseline of the measured spectra. Therefore, the line intensities were obtained from a fit of a line shape function to experimental spectra. A number of spectra (typically 8−10) were measured under identical conditions for the different R(2)-lines and averaged. From the intensity ratio of the transitions from K'' = 1 and K'' = 2 the rotational temperature could be determined, and the nuclear spin symmetry relaxation was investigated, comparing the intensities of the rovibrational transition from K'' = 0 and K'' = 1 and for K'' = 0 and K'' = 2, respectively.

4.2. Diode Laser Measurements of CHD_3. Diode laser spectra of the CH-stretching vibration ν_1 for CHD_3 were measured in the supersonic jet for the R(2)-lines around 3012 cm^{-1} and for the R(3)-lines around 3018 cm^{-1} (see Figures 4 and 5). In Figure 5 the jet spectra for the R(2)-lines of a mixture with x_{He} = 0.90 and x_{He} = 0.95 are compared with FTIR spectra measured in a low temperature cell at 80 K.[63] To allow for a better comparison, the FTIR spectra have been scaled by a factor of 0.022. Due to saturation effects the lines shown in the figure are considerably broadened; only the weaker lines of the FTIR spectra (not shown in the figure) have a line width close to the Doppler width of 0.0045 cm^{-1} with some small contributions from collisional broadening at a pressure of 500 Pa and from the spectral line shape function of the spectrometer. The weaker lines in the FTIR spectrum arise from levels with higher rotational quantum numbers from higher vibrational levels which are absent under molecular beam conditions. As the beam of the diode laser is perpendicular to the molecular expansion, a line width below 0.002 cm^{-1} is expected, whereas the width of the averaged diode laser spectra is larger by a factor of 3−4. This increase of the line width is to a large part due to the averaging process, arising from uncertainties of the spectral calibration of each

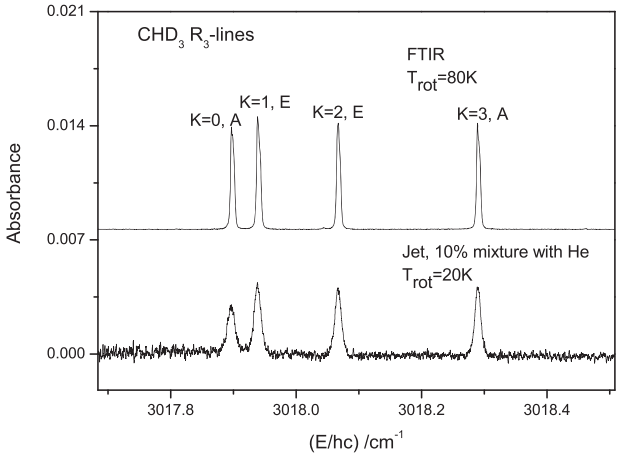

Figure 4. IR spectra as Napierian absorbance $\ln(I_0/I)$ for the R(3)-lines of the ν_1 fundamental in CHD_3. Upper trace: FTIR spectra at 80 K in a cooling cell with a path length of 5 m and a total pressure of 500 Pa (He/CHD_3), recorded with an instrumental bandwidth of 0.0027 cm^{-1}. Lower trace: Diode laser spectrum in a molecular beam (x_{He} = 0.90, T_{rot} = 20 K). The FTIR spectrum is scaled by a factor 0.001 to show an absorbance comparable to the diode laser spectrum (see also ref 63).

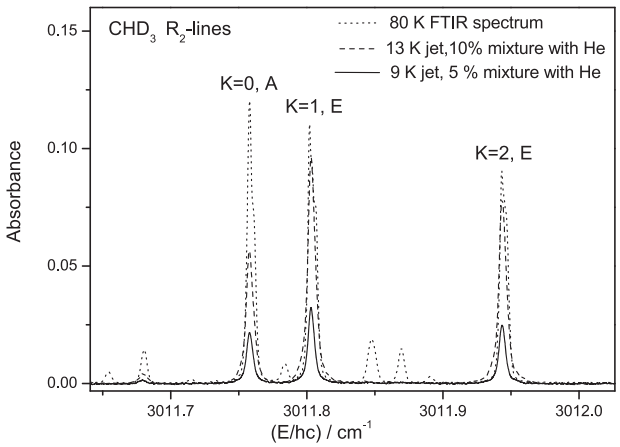

Figure 5. IR spectra as Napierian absorbance $\ln(I_0/I)$ for the R(2)-lines of the ν_1 fundamental in CHD_3. FTIR spectrum at 80 K measured in a cooling cell with a path length of 5 m and a total pressure of 500 Pa (He/CHD_3, ···); diode laser spectra in a molecular beam (x_{He} = 0.90, T_{rot} = 13 K, ---; x_{He} = 0.95, T_{rot} = 9 K, —). Instrumental bandwidth for the FTIR spectra: 0.0027 cm^{-1} (fwhm). The FTIR spectrum is scaled by a factor of 0.022 to show an absorbance comparable to the diode laser spectra.

DOI: 10.1021/acs.jpca.9b02580
J. Phys. Chem. A 2019, 123, 6160−6174

spectral scan, and to a small part due the laser line width. The shape of the measured spectral lines can be well-represented by the Lorentzian line shape function. While the limited effective resolution also limits the accuracy of absolute intensities, the effect on relative intensities is significantly smaller as estimated from simulations. This is also confirmed by the higher resolution measurements with the IR-OPO. Figure 6 shows

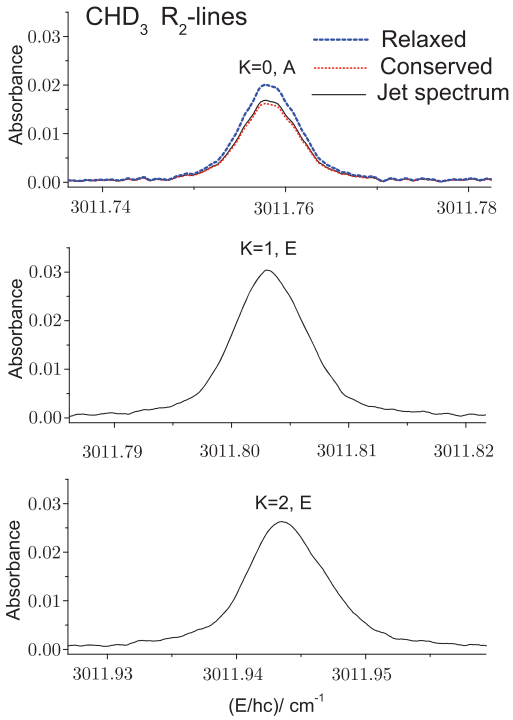

Figure 6. Measured spectral line shape as Napierian absorbance $\ln(I_0/I)$ for the R(2)-lines of ν_1 of CHD_3 (—) for x_{He} = 0.95. From the intensity ratio of the K = 1 and K = 2 lines, a rotational temperature of T_{rot} = 9.7 K is obtained. From these intensity ratios the absorption spectrum for the K = 0 line is calculated assuming complete nuclear spin symmetry conservation (··· red, almost coinciding with the experiment) and perfect nuclear spin symmetry relaxation (--- blue).

an enlarged view of the measured spectra of the three R(2)-lines. From the temperature derived from the intensities of the K = 1 and K = 2 lines, the intensity of the K = 0 line is calculated for complete nuclear spin symmetry conservation (dotted line red) and complete nuclear spin symmetry relaxation (dashed line blue). The experimental spectrum of the K = 0 line (solid line) is quite close to the spectrum calculated for complete nuclear spin symmetry conservation. To investigate to what extent the nuclear spin symmetry is conserved during the formation of the molecular beam, the expected relative line intensities of the different rovibrational lines were calculated as a function of the rotational temperature for the two limiting cases: for perfect nuclear spin symmetry conservation and for complete nuclear spin symmetry relaxation. As in the experiments no absolute line intensities can be measured, the ratios of the line intensity for K = 0 to the line intensities for K = 1 and K = 2 are plotted as a function of temperature for the R(2)-lines in Figure 7 and for the R(3)-lines in Figure 8. The molecular parameters, the energies of the rotational levels of the vibrational ground state E_{JK}, the Hönl–London factors A_{KJ}, and the spin statistical

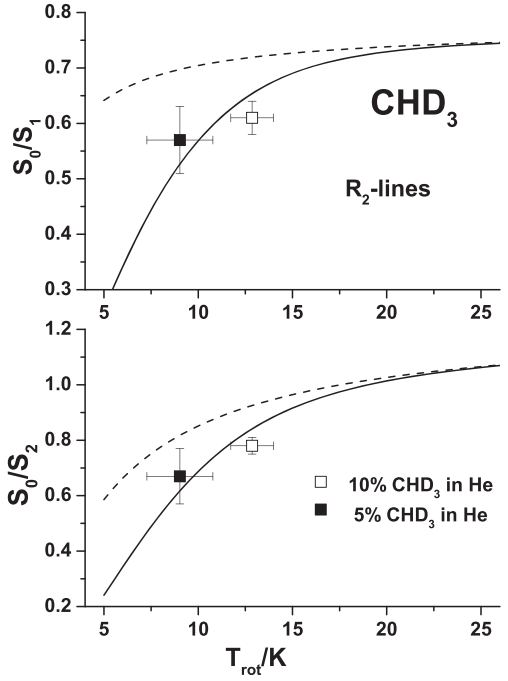

Figure 7. Calculated ratio of the R(2)-lines intensities in CHD_3, where the line intensity of K = 0 is divided by the line intensity of K = 1 (upper part) and K = 2 (lower part) as a function of the rotational temperature for perfect nuclear spin symmetry conservation (full line) and complete nuclear spin symmetry relaxation (dashed line). Included in the diagram are the experimental data points for different CHD_3/He-mixtures: (□) x_{He} = 0.90, (■) x_{He} = 0.95.

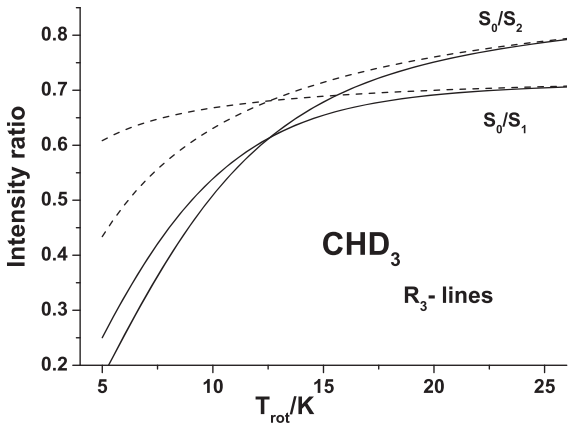

Figure 8. Calculated ratio of the line intensities for K = 0 divided by line intensities for K = 1 (S_0/S_1 and K = 2 (S_0/S_2) of the R(3)-lines of ν_1 in CHD_3 as a function of the rotational temperature for perfect nuclear spin symmetry conservation (full lines) and complete nuclear spin symmetry relaxation (dashed lines).

weight $g_I(\Gamma)$, which are necessary to calculate the relative line intensities, are summarized for CHD_3 and CH_3D together with the spectral line wavenumbers used in the measurement in Table 4. From Figures 7 and 8, it is clearly visible that rotational temperatures below 20 K have to be obtained in the molecular beam to decide to which extent the nuclear spin is conserved during the molecular beam expansion.

Absorption spectra of the R(2)-lines were measured in the molecular beam for two different mixtures with x_{He} = 0.90 and

DOI: 10.1021/acs.jpca.9b02580
J. Phys. Chem. A 2019, 123, 6160–6174

Table 4. Parameters To Calculate the Relative Line Intensities for the R(2)- and R(3)-Lines of the ν_1 Fundamental in CHD_3 and CH_3D[a]

			CHD_3						
			R_2-lines						
J'	J''	K	A_{KJ}	g_I	N_K	$\tilde{\nu}''/cm^{-1}$	$\tilde{\nu}_{trans}/cm^{-1}$	p_c^{rel}(10 K)	p_c^{rel}(20 K)
3	2	0	9/15	11	1	19.673	3011.75864	0.02766	0.04837
3	2	1	8/15	8	2	19.023	3011.80076	0.04873	0.06646
3	2	2	5/15	8	2	17.073	3011.94203	0.04032	0.04779
			R_3-lines						
J'	J''	K	A_{KJ}	g_I	N_K	$\tilde{\nu}''/cm^{-1}$	$\tilde{\nu}_{trans}/cm^{-1}$	p_c^{rel}(10 K)	p_c^{rel}(20 K)
4	3	0	16/28	11	1	39.343	3017.89502	0.00218	0.01567
4	3	1	15/28	8	2	38.693	3017.93886	0.00404	0.02270
4	3	2	12/28	8	2	36.744	3018.0638	0.00428	0.02090
4	3	3	7/28	11	2	33.494	3018.28679	0.00442	0.02088
			CH_3D						
			R_2-lines						
J'	J''	K	A_{KJ}	g_I	N_K	$\tilde{\nu}''/cm^{-1}$	$\tilde{\nu}_{trans}/cm^{-1}$	p_c^{rel}(10 K)	p_c^{rel}(20 K)
3	2	0	9/15	4	1	23.279	2993.355593	0.02428	0.06743
3	2	1	8/15	2	2	24.649	2993.258434	0.03691	0.06487
3	2	2	5/15	2	2	28.760	2992.918724	0.01277	0.03016

[a]The rotational energies of E_{JK} were calculated for CHD_3 using rotational constants from refs 63 and 72 and the values for CH_3D from refs 71 and 81. $\tilde{\nu}''$ is the term value for the lower level, and $K = K'' = K'$. The last columns give the relative population p_c^{rel} of the different levels, calculated for complete nuclear spin symmetry conservation at T = 10 and 20 K.

x_{He} = 0.95 (see Figure 5). To obtain a reliable value for T_{rot}, the rotational temperature was determined for a number of measured spectra from the intensity ratio of the K = 1 and K = 2 lines, averaged over all measured spectra. A rotational temperature of T_{rot} = (12.9 ± 1.1 K) for the sample with the high concentration (10% CHD_3) and T_{rot} = (9.0 ± 1.6 K) for the sample with the low concentration (5% CHD_3) was determined. The rotational temperatures of R(2)-lines are low enough to determine the degree of nuclear spin symmetry relaxation during the molecular beam expansion which is obtained from the ratios for the intensities of the K = 0 line divided through the intensities of the K = 1 and K = 2 lines, respectively. These ratios are included in the theoretical diagrams in Figure 7 for the two different expansion conditions. They are found close to the intensity ratios expected for complete spin symmetry conservation at the temperature considered.

In an additional experiment, an attempt was made to determine the degree of nuclear spin symmetry conservation during the expansion also for the R(3)-transitions. Figure 4 shows a comparison of the scaled FTIR spectrum measured at 80 K and the diode laser spectra from the molecular beam. In Figure 9, the relative line intensities obtained in the molecular beam for the R(3)-lines for x_{He} = 0.90 are shown on a logarithmic scale as a function of their ground state energy. The measured spectra were averaged over 8 scans (measured at different time), and the line intensities were obtained from the integration of the final spectrum. Within the uncertainty all the points for K = 0 to K = 3 are found to fall on a straight line resulting in a rotational temperature of 18.7 ± 0.8 K. This rotational temperature is already close to the limit where the difference of the intensity ratios is too small to determine the degree of nuclear spin symmetry relaxation for our experimental accuracy. The rotational temperature obtained for x_{He} = 0.90 on the R(3)-lines is slightly higher than the one obtained for the R(2)-lines. One reason is the lower backing pressure of 1 bar, and an additional reason could result from

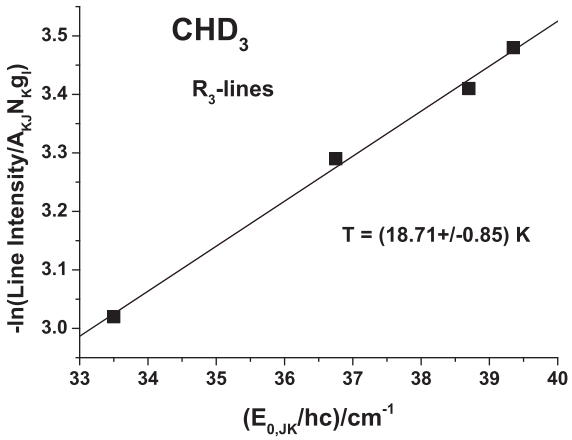

Figure 9. Logarithmic diagram of the measured line intensities for the different K-lines of the R(3)-transition of ν_1 in CHD_3 as a function of the rotational energy in the vibrational ground state. A rotational temperatures of 18.7 ± 0.8 K is derived from a linear fit. The line intensities for the determination of the rotational temperature were determined from a fit of a spectrum obtained as an average value of all measured spectra.

the unstable expansion conditions of the slit nozzle. An attempt was made to measure the R(3)-lines also for a smaller mole fraction of CHD_3 (x_{He} = 0.95) in the mixture. Unfortunately, as the line intensities for the R(3)-lines drop by nearly 1 order of magnitude when reducing the rotational temperature from 20 to 10 K, the signal-to-noise ratio was too low to derive reliable line intensities and to determine the degree of nuclear spin symmetry relaxation for these experimental conditions.

Figure 9 demonstrates in an exemplary fashion that the experimental results agree well with the assumption of a Boltzmann distribution for the rotational levels (except for nuclear spin symmetry conservation). This is in agreement

DOI: 10.1021/acs.jpca.9b02580
J. Phys. Chem. A 2019, 123, 6160−6174

with findings on $^{12}CH_4$, $^{13}CH_4$, and other molecules where this has been studied (see refs 23, 27, 28, 31, 33, and 45−47, for example). Indeed, this finding is the rule rather than the exception. As discussed in ref 45, while non-Boltzmann effects might exist, in principle, for higher levels, these are so weakly populated that their overall contribution to the relative concentrations of the nuclear spin isomers is sufficiently small, such that the corresponding uncertainty is less than the uncertainty in the experimental intensities of the strong lines used in the analysis. Such possible non-Boltzmann populations in the higher levels therefore do not affect the conclusions on nuclear spin symmetry conservation.

4.3. Diode Laser Measurements of CH_3D. Spectra for CH_3D were measured in the molecular beam on the R(2)-lines of the CH-stretching fundamental around 2993 cm^{-1} (Table 4) for two different mixtures with x_{He} = 0.90 and x_{He} = 0.95. The molecular beam spectra are shown together with a scaled FTIR spectrum at 80 K in Figure 10. As can be seen from

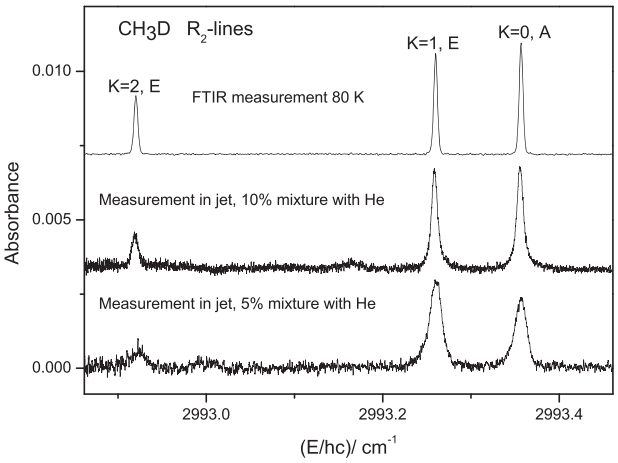

Figure 10. IR spectra of the R(2)-lines of the ν_1 fundamental in CH_3D. Upper trace: FTIR spectrum at 80 K measured in a cooling cell with a path length of 5 m and a total pressure of 500 Pa (He/CHD_3), recorded with an instrumental bandwidth of 0.0027 cm^{-1} (fwhm). Middle trace: Diode laser spectrum as Napierian absorbance $\ln(I_0/I)$ in a molecular beam (x_{He} = 0.90, T_{rot} = 10 K). Lower trace: Diode laser spectrum as Napierian absorbance in a supersonic expansion (x_{He} = 0.95, T_{rot} = 7 K, average of 4 spectra). The FTIR spectrum is scaled by a factor of 0.002 to show an absorbance comparable to the diode laser spectra.

Figure 10, the K = 2 line is weak. This is quite crucial as an incorrect determination of its line intensity can lead to an incorrect determination of T_{rot} of the spectra. From the measured spectra a rotational temperature T_{rot} = 9.93 ± 1.45 K was obtained for x_{He} = 0.90 and T_{rot} = 7.66 ± 1.64 K for x_{He} = 0.95, respectively.

Figure 11 shows the theoretical intensity ratios for the R(2)-lines of CH_3D as a function of the rotational temperature for the two limiting cases of perfect nuclear spin symmetry conservation and complete nuclear spin symmetry relaxation. Due to the different rotational constants the calculated intensity ratios for the two relaxation scenarios are well-distinguished for low rotational temperatures up to 25 K. The experimental intensity ratios determined for two different expansion conditions are also included in the figures. They would indicate a strong contribution from nuclear spin symmetry relaxation during the expansion. This result is

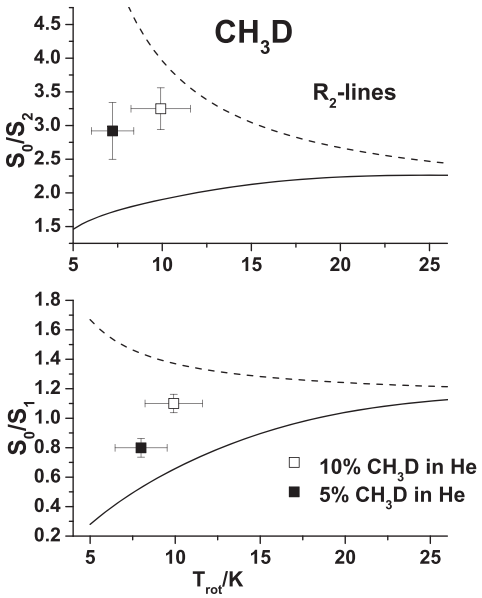

Figure 11. Calculated ratio of the line intensities for K = 0 divided by K = 1 (upper part) and K = 2 (lower part) of the R(2)-lines of ν_1 in CH_3D as a function of the rotational temperature for perfect nuclear spin symmetry conservation (full line) and complete nuclear spin symmetry relaxation (dashed line). Included in the diagram are experimental data points for different CH_3D/He-mixtures: (□) x_{He} = 0.90, (■) x_{He} = 0.95.

quite unexpected as for similar molecules complete nuclear spin symmetry conservation has been found for the expansion in a molecular beam (see OPO experiments below and refs 27 and 31). The degree of nuclear spin symmetry relaxation derived from the ratio of the line intensities depends strongly on the rotational temperature derived from the intensity rations of the K = 1 and K = 2 lines. If the measured intensity of the K = 2 lines is too small, the apparent rotational temperature derived is reduced and the experimental data points in Figure 11 are shifted to the left to lower apparent temperatures, suggesting a stronger contribution of nuclear spin symmetry relaxation. An additional problem may be found in the experimental technique: Scanning the diode laser during the molecular gas pulse has one important drawback. Reliable line intensities are only obtained if the particle density in the molecular beam is constant during the complete laser scan. If spectral lines are measured toward the end of the gas pulse the molecular density might be reduced, resulting in an absorption cross section that is too small and a rotational temperature that is too small. As a result of the applied current ramp, the emission wavelength of the diode laser increases with time and the low frequency lines are measured toward the end of the scan. For CH_3D the wavenumber of the K = 2 line is shifted by 0.4 cm^{-1} to lower values as compared to the close lying K = 1 and K = 0 lines, and there is a risk that the K = 2 line is measured already in the part of the molecular pulse with reduced particle density. This would result in an incorrect apparent rotational temperature that is too low and could explain the apparently high contributions of nuclear spin symmetry relaxation found in the diode laser experiments for CH_3D. A reduction of the particle density in the molecular beam of 27% shifts the rotational temperature from 13 K to the apparent experimental value of T_{rot} = 7.65 K. However, for a

DOI: 10.1021/acs.jpca.9b02580
J. Phys. Chem. A 2019, 123, 6160−6174

Table 5. Line Positions for the R(2)-Lines of ν_1 in CH_3F, $CH_3{}^{35}Cl$, and CH_3D Measured with the Comb Referenced OPO and Comparison with Line Position from FTIR Spectra and Published Literature Data[a]

molecule	J''	K''	J'	K'	$\Gamma_{rve}(C_{3v})$	$\Gamma_{ns}(S_3^*)$	$\tilde{\nu}_{0,OPO}/cm^{-1}$	$\tilde{\nu}_{0,FTIR}/cm^{-1}$	$\tilde{\nu}_{0,lit.}/cm^{-1}$
CH_3F	2	0	3	0	A_1	A_1^+	2868.33085(2)		2868.3318[83]
	2	1	3	1	E	E^+	2868.31155(2)		2868.3125[83]
	2	2	3	2	E	E^+	2868.25336(1))		2868.2542[83]
$CH_3{}^{35}Cl$	2	0	3	0	A_1	A_1^+	2970.42925(3)		2970.4293[84]
	2	1	3	1	E	E^+	2970.37368(2)		2970.3735[84]
	2	2	3	2	E	E^+	2970.20705(2)		2970.2072[84]
CH_3D	2	0	3	0	A_1	A_1^+	2993.35584(2)	2993.35673	2993.355593[81]
	2	1	3	1	E	E^+	2993.25895(1)	2993.25987	2993.258434[81]
	2	2	3	2	E	E^+	2992.91940(4)	2992.92020	2992.918724[81]

[a]The uncertainty of the OPO line positions (value in parentheses) is given for a level of confidence of 95%. The $\Gamma_{rve}(C_{3v})$ gives the symmetry species of the rovibronic wavefunction (rve) in C_{3v} and $\Gamma_{ns}(S_3^*)$, the symmetry species of the nuclear spin wave function (ns) allowed with the corresponding rve species.

rotational temperature of 13 K the measured intensity ratios of the $K = 1$ and $K = 0$ lines would correspond to perfect nuclear spin symmetry conservation. Thus, the results from the diode laser measurements on CH_3D are ambiguous, and we decided to complement them with IR/OPO measurements.

4.4. IR-OPO Measurements for CH_3D, CH_3F, and $CH_3{}^{35}Cl$. To answer the question regarding whether during the expansion nuclear spin relaxation effects are important for CH_3D and to increase our molecular database, additional experiments have been performed using the idler radiation of a continuous wave IR-OPO as a light source. As for the diode laser experiments, the intensities of the R(2)-lines of the symmetric CH-stretching vibration ν_1 were measured for CH_3D and also for $CH_3{}^{35}Cl$, and of the $2\nu_5^0$ mode (BB mode in the notation of Graner and Guelachvili[83]) for CH_3F with the OPO setup (see Table 5). For the expansion the mole fraction of the compounds studied was varied from $x_{CH_3X} = 0.025$ to 0.05 and He or Ar was used as a carrier gas with a backing pressure of up to 2 bar. Under these experimental conditions the rotational temperature could be varied from $T_{rot} = 7$ to 27 K for CH_3D and from 11 to 18 K for $CH_3{}^{35}Cl$ and CH_3F. The measured rotational transitions are summarized in Table 5 together with their transition wavenumbers derived from the spectra where the IR-OPO has been locked to the frequency comb together with published data from the literature. The uncertainty in the absolute values of the transition wavenumbers depends more on the angle between the molecular beam and the laser beam than on the uncertainty in the laser frequency (approximately 100 kHz). A deviation of 1° from a perpendicular intersection would result in a frequency shift of approximately 3 MHz for the applied experimental conditions. Assuming a precision of the measured angle of intersection of ±2° results in an uncertainty of the measured transition frequencies of ±6 MHz. Segments of the measured molecular beam spectra of CH_3D, CH_3F and $CH_3{}^{35}Cl$ are shown in Figures 12−14.

In Figure 15 the calculated intensity ratios for the $K = 0$ and $K = 1$ lines are shown for the molecules studied as a function of the rotational temperature for the limiting cases of perfect nuclear spin symmetry conservation and complete nuclear spin symmetry relaxation, together with the intensity ratios for the different expansion conditions. For CH_3Cl and CH_3F no indication of a contribution of nuclear spin symmetry relaxation is found. The experimental intensity ratios are situated with one exception close to or below the theoretical values for complete nuclear spin symmetry conservation. Only

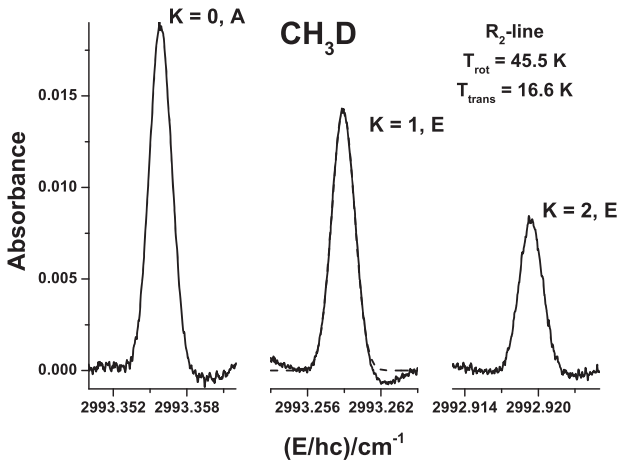

Figure 12. IR spectrum as Napierian absorbance $\ln(I_0/I)$ for the R(2)-lines of the ν_1 fundamental in CH_3D measured with the comb referenced OPO with an effective bandwidth of $\Delta\tilde{\nu}_{OPO} = 3 \times 10^{-5}$ cm^{-1}. The spectrum was recorded in a seeded molecular beam with $x_{He} = 0.975$ and a distance of 2 mm from the nozzle. From the intensity distribution, a rotational temperature of $T_{rot} = 45.5$ K is obtained; a fit of Gaussian distribution to the $K = 1$ line (dashed line) results in a "translational temperature" of $T_{trans} = 16.6$ K.

for CH_3D are the experimental ratios found predominantly above the theoretical values for complete nuclear spin symmetry conservation, and a contribution from nuclear spin symmetry relaxation cannot be completely excluded, which would be consistent with the less secure results from the diode laser measurements. Nevertheless, the IR/OPO results for CH_3D are clearly still consistent with nuclear spin symmetry conservation, and any contribution from nuclear spin symmetry relaxation must be minor under these conditions. The experimental uncertainties are much smaller for the IR/OPO data than for the diode laser measurements, and thus, we rely in our conclusions rather than on our OPO results.

5. DISCUSSION AND CONCLUSIONS

While for a long time the conservation of nuclear spin symmetry under conditions where inelastic collisions occur was taken for granted, for example in the area of molecular spectroscopy,[11,18,19] it has been clear from the pioneering work of Curl, Kasper, and Pitzer[18] that conversion between nuclear spin isomers is possible. Since that time it has been understood that the mechanisms of nuclear spin symmetry change by

DOI: 10.1021/acs.jpca.9b02580
J. Phys. Chem. A 2019, 123, 6160−6174

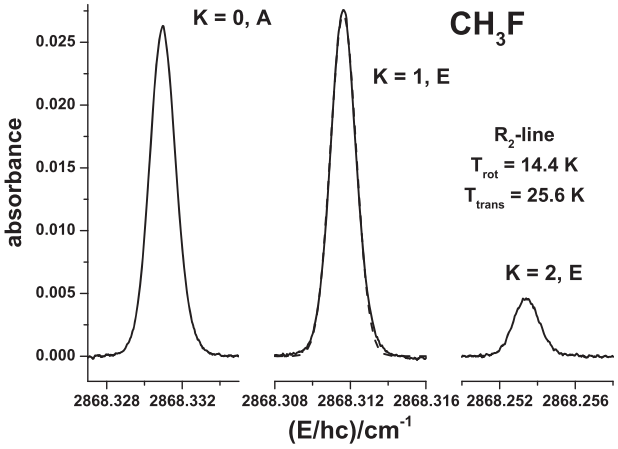

Figure 13. IR spectrum as Napierian absorbance $\ln(I_0/I)$ for the R(2)-lines of the $2\nu_5$ fundamental in CH_3F measured with the comb referenced OPO with an effective bandwidth of $\Delta\tilde{\nu}_{OPO} = 3 \times 10^{-5}$ cm^{-1}. The spectrum was recorded in a seeded molecular beam with $x_{He} = 0.975$ and a distance of 4 mm from the nozzle. From the intensity distribution, a rotational temperature of $T_{rot} = 14.4$ K is obtained; a fit of Gaussian distribution to the $K = 1$ line (dashed line) results in a "translational temperature" of $T_{trans} = 25.6$ K.

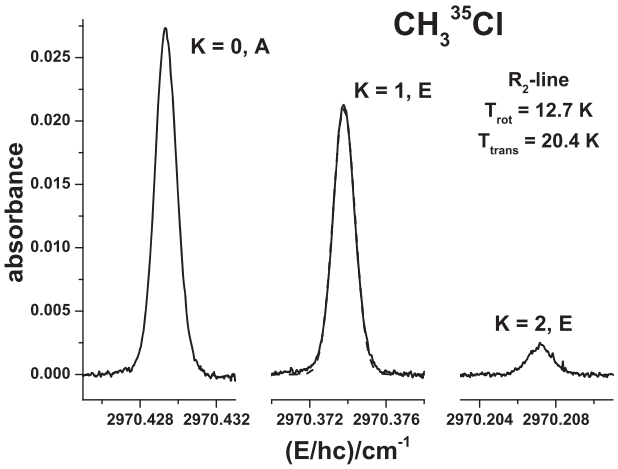

Figure 14. IR spectrum as Napierian absorbance $\ln(I_0/I)$ for the R(2)-lines of the ν_1 fundamental in $CH_3{}^{35}Cl$ measured with the comb referenced OPO with an effective bandwidth of $\Delta\tilde{\nu}_{OPO} = 3 \times 10^{-5}$ cm^{-1}. The spectrum was recorded in a seeded molecular beam with $x_{He} = 0.975$ and a distance of 10 mm from the nozzle. From the intensity distribution, a rotational temperature of $T_{rot} = 12.7$ K is obtained; a fit of Gaussian distribution to the $K = 1$ line (dashed line) results in a "translational temperature" of $T_{trans} = 20.4$ K.

inelastic collisions depend on the detailed structure of the molecular spectra, with the symmetry of the molecules allowing for certain preferred degeneracies, and also details of the nuclear spin rotation and spin−spin couplings. Thus, there is considerable interest in studying, say, isotopomers of polyatomic molecules differing by their symmetries and rotational−vibrational level distribution in order to gain insight into the broader phenomenology of these processes, about which only rather limited knowledge is available until today.

We have studied in the present work the question of nuclear spin symmetry conservation (or relaxation) for the symmetric top molecules CHD_3, CH_3D, CH_3F, and CH_3Cl during He

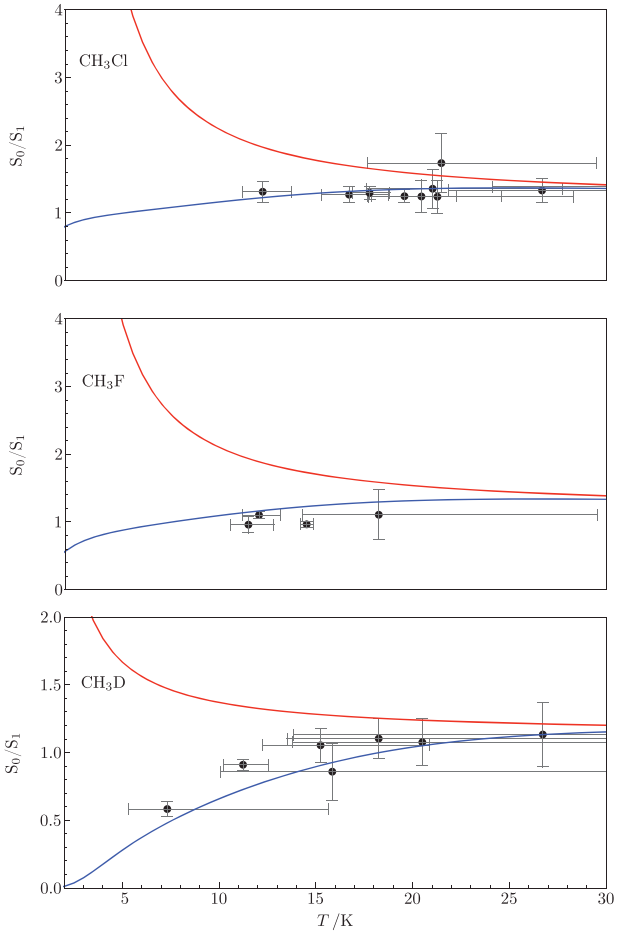

Figure 15. Calculated (lines) and experimental (points) ratios S_0/S_1 of the intensities of the $K = 0$ and $K = 1$ lines as a function of the rotational temperature for $CH_3{}^{35}Cl$, CH_3F, and CH_3D. The upper function (red) corresponds to complete nuclear spin symmetry relaxation whereas the lower function (blue) represents the calculated ratio for perfect nuclear spin symmetry conservation.

and Ar seeded supersonic jet expansions for the first time. In these molecules one has two nuclear spin isomers, which can be labeled as A and E isomers according to their rovibrational symmetry species (the electronic ground state being totally symmetric). The infrared absorption spectra around 3000 cm^{-1} were measured at high resolution with two different laser radiation sources: a tunable diode laser and a continuous wave infrared OPO frequency locked to a frequency comb. With changes in the backing pressure of the carrier gas (He and Ar) and the mixing ratio ($x_{CH_3X} = 0.025-0.1$), rotational temperatures T_{rot} between 7 and 27 K were reached. These rotational temperatures are low enough to determine the degree of nuclear spin symmetry relaxation during the expansion. The comparison of the experimental ratios of the line intensities for the A nuclear spin isomers with ($K = 0, 3...$) and the E nuclear spin isomers with ($K = 1, 2, 4...$) with the calculated ratios for a given rotational temperature shows that for CHD_3, CH_3F, and CH_3Cl nuclear spin symmetry relaxation is absent or of minor importance under the conditions of the present experiment. For CH_3D the situation is less clear. From the experiments with the OPO a small contribution from nuclear spin symmetry relaxation cannot completely be

DOI: 10.1021/acs.jpca.9b02580
J. Phys. Chem. A 2019, 123, 6160−6174

excluded, whereas the less reliable diode laser experiments suggest a more significant contribution from nuclear spin symmetry relaxation but have a large uncertainty. Thus, even for CH_3D the results are consistent with nuclear spin symmetry conservation within the large experimental uncertainties.

In a discussion of the possibilities for nuclear spin symmetry conversion in supersonic jet expansions, the two main mechanisms of the intramolecular quantum relaxation in the monomer[18,26,41,45] or by cluster formation[47] should be considered. In the present experiment the formation of clusters $(CH_3X)_n$ or $(CHD_3)_n$ is not too important, as has been studied in detail for similar conditions of seeded supersonic expansions of the normal isotopmers of CH_4,[31,33] and the exchange of protons within the cluster is highly unlikely. Thus, our results on nuclear spin symmetry conservation are consistent with the expectation of only a small effect from the intramolecular quantum relaxation mechanism. The results on CH_3D may deserve further attention. Also, the complexity of the CHD_3 sublevel structure in the A and E nuclear spin isomers raises the question of nuclear spin symmetry conversion within the substructure which contains different nuclear spin isomers (Section 3.1). Investigation of such effects would be possible with studies at hyperfine resolution,[61] which remain a task for the future.

AUTHOR INFORMATION

Corresponding Author

*E-mail: Martin@Quack.ch. Phone: +41 44 632 44 21. Fax: +41 44 632 10 21.

ORCID

Martin Quack: 0000-0002-1351-8584

Notes

The authors declare no competing financial interest.

ACKNOWLEDGMENTS

Our work is supported financially by the ETH Zürich (in particular the Laboratory for Physical Chemistry) and the Schweizerischer Nationalfonds, as well as an ERC Advanced Grant and COST MOLIM. We are grateful to S. Albert, Z. Guennoun, F. Merkt, E. Miloglyadov, and in particular G. Wichmann for help, support, and discussions, and we thank Andreas Schneider, Andres Laso, and Eduard Peyer for very important technical support.

REFERENCES

(1) Reid, S. A.; Winterbottom, F.; Scott, D. C.; de Juan, J.; Reisler, H. A Crossed Beam Study of the Reaction $C(^3P) + N_2O$: Energy Partitioning Between $NO(X^2\Pi)$ and $CN(X^2\Sigma^+)$ Products. *Chem. Phys. Lett.* **1992**, *189*, 430−436.

(2) Reid, S. A.; Reisler, H. Experimental Studies of Resonances in Unimolecular Decomposition. *Annu. Rev. Phys. Chem.* **1996**, *47*, 495−525.

(3) Scholefield, M. R.; Choi, J. H.; Goyal, S.; Reisler, H. Endoergic Reactions of Hyperthermal $C(^3P)$ with Methane and Acetylene. *Chem. Phys. Lett.* **1998**, *288*, 487−493.

(4) Fedorov, I.; Koziol, L.; Mollner, A. K.; Krylov, A. I.; Reisler, H. Multiphoton Ionization and Dissociation of Diazirine: A Theoretical and Experimental Study. *J. Phys. Chem. A* **2009**, *113*, 7412−7421.

(5) Rocher-Casterline, B. E.; Mollner, A. K.; Ch'ng, L. C.; Reisler, H. Imaging H_2O Photofragments in the Predissociation of HCl - H_2O Hydrogen-Bonded Dimer. *J. Phys. Chem. A* **2011**, *115*, 6903−6909.

(6) Ch'ng, L. C.; Samanta, A. K.; Czakó, G.; Bowman, J. M.; Reisler, H. Experimental and Theoretical Investigations of Energy Transfer and Hydrogen-Bond Breaking in the Water Dimer. *J. Am. Chem. Soc.* **2012**, *134*, 15430−15435.

(7) Ch'ng, L. C.; Samanta, A. K.; Wang, Y.; Bowman, J. M.; Reisler, H. Experimental and Theoretical Investigations of the Dissociation Energy E_0 and Dynamics of the Water Trimer $(H_2O)_3$. *J. Phys. Chem. A* **2013**, *117*, 7207−7216.

(8) Samanta, A. K.; Ch'ng, L. C.; Reisler, H. Imaging Bond Breaking and the Vibrational Energy Transfer in Small Water Containing Clusters. *Chem. Phys. Lett.* **2013**, *575*, 1−11.

(9) Zuraski, K.; Kwasniewski, D.; Samanta, A. K.; Reisler, H. Vibrational Predissociation of the HCl-$(H_2O)_3$ Tetramer. *J. Phys. Chem. Lett.* **2016**, *7*, 4243−4247.

(10) Shuler, K. E. Adiabatic Correlation Rules for Reactions Involving Polyatomic Intermediate Complexes and their Application to the Formation of $OH(^2\Sigma^+)$ in the H_2-O_2 Flame. *J. Chem. Phys.* **1953**, *21*, 624−632.

(11) Herzberg, G. *Molecular Spectra and Molecular Structure, I. Spectra of Diatomic Molecules*; D. Van Nostrand: New York, 1950.

(12) Woodward, R. B.; Hoffmann, R. *The Conservation of Orbital Symmetry*; Verlag Chemie: Weinheim, 1970.

(13) Quack, M. In *Handbook of High Resolution Spectroscopy; Fundamental Symmetries and Symmetry Violations from High Resolution Spectroscopy*; Quack, M., Merkt, F., Eds.; Wiley: Chichester, NY, 2011; Vol. *1*, Chapter 18, pp 659−722.

(14) Quack, M. Detailed Symmetry Selection-Rules for Reactive Collisions. *Mol. Phys.* **1977**, *34*, 477−504.

(15) Bonhoeffer, K. F.; Harteck, P. Experimente über Para- und Orthowasserstoff. *Naturwissenschaften* **1929**, *17*, 182.

(16) Mecke, R. Intensitätswechsel im Rotationsschwingungsspektrum des Wasserdampfes. (Ortho- und Para-Wasser). *Naturwissenschaften* **1932**, *20*, 657.

(17) Mecke, R.; Baumann, W. Das Rotationsschwingungsspektrum des Wasserdampfes. *Phys. Z.* **1932**, *33*, 833−835.

(18) Curl, R. F.; Kasper, J. V. V.; Pitzer, K. Nuclear Spin State Equilibrium through Nonmagnetic Collisions. *J. Chem. Phys.* **1967**, *46*, 3220−3228.

(19) Herzberg, G. *Molecular Spectra and Molecular Structure, II. Infrared and Raman Spectra of Polyatomic Molecules*; D. Van Nostrand: New York, 1945.

(20) Herzberg, G. *Molecular Spectra and Molecular Structure, III. Electronic Spectra and Electronic Structure of Polyatomic Molecules*; D. Van Nostrand: New York, 1966.

(21) Oka, T. Collision-Induced Transitions between Rotational Levels. *Adv. At. Mol. Phys.* **1974**, *9*, 127−206.

(22) Merkt, F.; Quack, M. In *Handbook of High-Resolution Spectroscopy; Molecular Quantum Mechanics and Molecular Spectra, Molecular Symmetry, and Interaction of Matter with Radiation*; Quack, M., Merkt, F., Eds.; Wiley: Chichester, NY, 2011; Vol. *1*, Chapter 1, pp 1−55 (see also preface to this handbook).

(23) Dübal, H. R.; Quack, M.; Schmitt, U. High-Resolution Interferometric Infrared-Spectroscopy of CO_2 and CH_4 Vapor at Low-Temperatures near 10 K—Collisional Cooling in Supersonic Jets and Nuclear Spin Symmetry Conservation. *Chimia* **1984**, *38*, 438−439.

(24) Uy, D.; Cordonnier, M.; Oka, T. Observation of Ortho-Para H_3^+ Selection Rules in Plasma Chemistry. *Phys. Rev. Lett.* **1997**, *78*, 3844−3847.

(25) Ernst, R. R.; Bodenhausen, G.; Wokaun, A. *Principles of Nuclear Magnetic Resonance in One and Two Dimensions*; Calderon Press: Oxford, 1987.

(26) Chapovsky, P.; Hermans, L. J. F. Nuclear Spin conversion in Polyatomic Molecules. *Annu. Rev. Phys. Chem.* **1999**, *50*, 315−345.

(27) Amrein, A.; Quack, M.; Schmitt, U. High-Resolution Interferometric Fourier Transform Infrared Absorption Spectroscopy in Supersonic Free Jet Expansions: Carbon Monoxide, Nitric Oxide, Methane, Ethyne, Propyne, and Trifluoromethane. *J. Phys. Chem.* **1988**, *92*, 5455−5466.

(28) Snels, M.; Horká-Zelenková, V.; Hollenstein, H.; Quack, M. In *Handbook of High Resolution Spectroscopy; High Resolution FTIR and*

DOI: 10.1021/acs.jpca.9b02580
J. Phys. Chem. A 2019, 123, 6160−6174

Diode Laser Spectroscopy of Supersonic Jets; Quack, M., Merkt, F., Eds.; Wiley: Chichester, NY, 2011; Vol. 2; Chapter 27, pp 1021−1067.
(29) Hepp, M.; Winnewisser, G.; Yamada, K. M. T. Conservation of the Nuclear Spin Modification of CH_4 in the Cooling Process by Supersonic Jet Expansion. *J. Mol. Spectrosc.* **1994**, *164*, 311−314.
(30) Miyamoto, Y.; Fushitani, M.; Ando, D.; Momose, T. Nuclear Spin Conversion of Methane in Solid Parahydrogen. *J. Mol. Spectrosc.* **1992**, *128*, 114502.
(31) Tanner, C. M.; Quack, M. Reinvestigation of the $\nu_2 + 2\nu_3$ Subband in the Overtone Icosad of $^{12}CH_4$ Using Cavity Ring-Down (CRD) Spectroscopy of a Supersonic Jet Expansion. *Mol. Phys.* **2012**, *110*, 2111−2135.
(32) Niederer, H. M.; Albert, S.; Bauerecker, S.; Boudon, V.; Seyfang, G.; Quack, M. On Nuclear Spin Symmetry Conservation in Methane. *Faraday Discuss.* **2011**, *150*, 128−130.
(33) Bjelobrk, Z.; Manca Tanner, C.; Quack, M. Investigation of the $\nu_2 + 2\nu_3$ Subband in the Overtone Icosad of $^{13}CH_4$ by Pulsed Supersonic Jet and Diode Laser Cavity Ring-Down Spectroscopy: Partial Rovibrational Analysis and Nuclear Spin Symmetry Conservation. *Z. Phys. Chem.* **2015**, *229*, 1575−1607.
(34) Chapovsky, P.; Cosléou, J.; Herlemont, F.; Khelkhal, M.; Legrand, J. Separation and Conversion of Nuclear Spin Isomers of Ethylene. *Chem. Phys. Lett.* **2000**, *322*, 424−428.
(35) Sun, Z.-D.; Takagi, K.; Matsushima, F. Separation and Conversion Dynamics of Four Nuclear Spin Isomers of Ethylene. *Science* **2005**, *310*, 1938−1941.
(36) Chapovsky, P. Hyperfine Spectra of CH_3F Nuclear Spin Conversion. *J. Phys. B: At., Mol. Opt. Phys.* **2000**, *33*, 1001−1011.
(37) Nagels, B.; Calas, N.; Roozemond, D. A.; Hermans, L. J. L.; Chapovsky, P. Level-Crossing Resonances in Nuclear Spin Conversion of Molecules. *Phys. Rev. Lett.* **1996**, *77*, 4732−4735.
(38) Chapovsky, P. Nuclear Spin Conversion in Formaldehyde. *J. Mol. Struct.* **2001**, *599*, 337−345.
(39) Peters, G.; Schramm, B. Nuclear Spin State Relaxation in Formaldehyde: Dependence of the Rate Constant on Pressure. *Chem. Phys. Lett.* **1999**, *302*, 181−186.
(40) Dickens, J. E.; Irvine, W. M. The Formaldehyde Ortho/Para ratio as a Probe of Dark Chemistry and Evolution. *Astrophys. J.* **1999**, *518*, 733−739.
(41) Miani, A.; Tennyson, J. Can Ortho-Para Transitions for Water Be Obeserved ? *J. Chem. Phys.* **2004**, *120*, 2732−2739.
(42) Limbach, H.-H.; Buntkowsky, G.; Matthes, J.; Gründemann, S.; Pery, T.; Walaszek, B.; Chaudret, B. Novel Insights into the Mechanism of Ortho/Para Spin Conversion of Hydrogen Pairs: Implication for Catalysis and Interstellar Water. *ChemPhysChem* **2006**, *7*, 551−554.
(43) Veber, S.; Bagryanskaya, E. G.; Chapovsky, P. L. On the Possibility of Enrichment of H_2O Nuclear Spin Isomers by Adsorption. *J. Exp. Theor. Phys.* **2006**, *102*, 76−83.
(44) Cacciani, P.; Coslèou, J.; Khelkhal, M. Nuclear Spin Conversion in H_2O. *Phys. Rev. A: At., Mol., Opt. Phys.* **2012**, *85*, 012521.
(45) Manca Tanner, C.; Quack, M.; Schmidiger, D. On Nuclear Spin Symmetry Relaxation in Supersonic Jets of H_2O. *Faraday Discuss.* **2011**, *150*, 118−122.
(46) Manca Tanner, C.; Quack, M.; Schmidiger, D. Nuclear Spin Symmetry Conservation and Relaxation in Water ($^1H_2\ ^{16}O$) Studied by Cavity Ring-Down (CRD) Spectroscopy of Supersonic Jets. *J. Phys. Chem. A* **2013**, *117*, 10105−10118.
(47) Manca Tanner, C.; Quack, M.; Schmidiger, D. Nuclear Spin Symmetry Conservation and Relaxation of Water ($^1H_2\ ^{16}O$) Seeded in Supersonic Jets of Argon and Oxygen: Measurements by Cavity Ring-Down Laser Spectroscopy. *Mol. Phys.* **2018**, *116*, 3718−3730.
(48) Tikhonov, V.; Volkov, A. Separation of Water into Its Ortho and Para Isomers. *Science* **2002**, *296*, 2363.
(49) Georges, R.; Michaut, X.; Moudens, A.; Goubet, M.; Pirali, O.; Soulard, P.; Huet, T.; Roy, P.; Fournier, M.; Vigasin, A.; Asselin, P. Nuclear Spin Symmetry Conservation in $^1H_2{}^{16}O$ investigated by direct absorption FTIR Spectroscopy of Water Vapor Cooled Down in Supersonic Expansions. *J. Phys. Chem. A* **2017**, *121*, 7455−7468.
(50) Votava, O.; Zelenkova, V.; Rakovsky, J. In *Proceedings of the 19th Symposium on Atomic, Cluster and Surface Physics 2018 (SASP 2018), Obergurgl, Austria, 11 to 16 February 2018*; Beyer, M., Wester, R., Scheier, P., Staud, I., Eds.; Innsbruck University Press (IUP): Innsbruck, 2018; pp 196−199.
(51) Albert, S.; Meier, B. H.; Quack, M.; Seyfang, G.; Trabesinger, A. On the Possibility of Stable Nuclear Spin Symmetry Isomers in H_2O. *Chimia* **2006**, *60*, 476.
(52) Tanaka, K.; Harada, M.; Tanaka, T.; Toshimitsu, M. Determination of the Proton Tunneling Splitting of the Vinyl Radical in the Ground State by Millimeter-Wave Spectroscopy Combined with Supersonic Jet Expansion and Ultraviolet Photolysis. *J. Chem. Phys.* **2004**, *120*, 3604−3618.
(53) Fushitani, M.; Momose, T. Nuclear Spin Selection Rules in the Photochemical Reaction of CH_3 in Solid Parahydrogen. *J. Chem. Phys.* **2002**, *116*, 10739−10743.
(54) Hippler, M.; Quack, M. High-Resolution Fourier Transform Infrared and cw-Diode Laser Cavity Ringdown Spectroscopy of the $\nu_2 + 2\nu_3$ Band of Methane near 7510 cm^{-1} in Slit Jet Expansions and at Room Temperature. *J. Chem. Phys.* **2002**, *116*, 6045−6055.
(55) Caviezel, M.; Quack, M.; Seyfang, G. High Resolution Diode Laser IR-Spectra Measured in a Pulsed Slit Nozzle Supersonic Jet Expansion. *Chimia* **2006**, *60*, 466.
(56) Horká-Zelenkova, V.; Caviezel, M.; Quack, M.; Seyfang, G. Test of Nuclear Spin Symmetry Conservation in Partially Deuterated Methane-Isotopmers in the Expansion of a Molecuar Supersonic Jet. *Chimia* **2010**, *64*, 568.
(57) He, Y.; Hollenstein, H.; Quack, M.; Richard, E.; Snels, M.; Bürger, H. High Resolution Analysis of the Complex Symmetric CF_3 Stretching Chromophore Absorption in CF_3I. *J. Chem. Phys.* **2002**, *116*, 974−983.
(58) Lovejoy, C. M.; Nesbitt, D. J. Slit Pulsed Valve for Generation of Long-Path-Length Supersonic Expansions. *Rev. Sci. Instrum.* **1987**, *58*, 807−811.
(59) Dietiker, P.; Quack, M.; Schneider, A.; Seyfang, G.; Uenlü, F. In *Proc. of the 17th SASP 2010*; Milewski, I., Kendl, A., Scheier, P., Eds.; Innsbruck University Press (IUP): Innsbruck, 2010; pp 161−164.
(60) Dietiker, P.; Miloglyadov, E.; Quack, M.; Schneider, A.; Seyfang, G. In *Proceedings of the 19th Symposium on Atomic, Cluster and Surface Physics 2014 (SASP 2014), Obergurgl, Austria, 8 to 14 February 2014*; Stock, D., Wester, R., Scheier, P., Eds.; Innsbruck University Press (IUP): Innsbruck, 2014; pp 226−229.
(61) Dietiker, P.; Miloglyadov, E.; Quack, M.; Schneider, A.; Seyfang, G. Infrared Laser Induced Population Transfer and Parity Selection in $^{14}NH_3$: A Proof of Principle Experiment Towards Detecting Parity Violation in Chiral Molecules. *J. Chem. Phys.* **2015**, *143*, 244305.
(62) Albert, S.; Bauerecker, S.; Quack, M.; Steinlin, A. Rovibrational Analysis of the $2\nu_3$, $3\nu_3$ and ν_1 bands of $CHCl_2F$ Measured at 170 and 298 K by High-Resolution FTIR Spectroscopy. *Mol. Phys.* **2007**, *105*, 541−558.
(63) Ulenikov, O. N.; Bekhtereva, E. S.; Albert, S.; Bauerecker, S.; Hollenstein, H.; Quack, M. High Resolution Infrared Spectroscopy and Global Vibrational Analysis for the CH_3D and CHD_3 Isotopomers of Methane. *Mol. Phys.* **2010**, *108*, 1209−1240.
(64) Longuet-Higgins, H. C. The Symmetry Group of Non-Rigid Molecules. *Mol. Phys.* **1963**, *6*, 445−461.
(65) Pepper, M. J. M.; Shavitt, I.; von Ragué Schleyer, P.; Glukhovtsev, M. N.; Janoschek, R.; Quack, M. Is the Stereomutation of Methane Possible? *J. Comput. Chem.* **1995**, *16*, 207−225.
(66) Marquardt, R.; Quack, M. Global Analytical Potential Hypersurfaces for Large Amplitude Nuclear Motion and Reactions in Methane. I. Formulation of the Potentials and Adjustment of Parameters to Ab Initio Data and Experimental Constraints. *J. Chem. Phys.* **1998**, *109*, 10628−10643. 27 Pages of Supporting Information Published as AIP Document No PAPS JCPS A6-109-010845 by

DOI: 10.1021/acs.jpca.9b02580
J. Phys. Chem. A 2019, 123, 6160−6174

American Institute of Physics, Physics Auxiliary Publication Service, Woodbury, NY, pp 1179−29999.
(67) Hollenstein, H.; Marquardt, R.; Quack, M.; Suhm, M. A. Dipole-Moment Function and Equilibrium Structure of Methane in an Analytical, Anharmonic 9-Dimensional Potential Surface Related to Experimental Rotational-Constants and Transition Moments by Quantum Monte-Carlo Calculations. *J. Chem. Phys.* **1994**, *101*, 3588−3602.
(68) Marquardt, R.; Quack, M. In *Handbook of High-Resolution Spectroscopy; Global Analytical Potential Energy Surfaces for High Resolution Molecular Spectroscopy and Reaction Dynamics*; Quack, M., Merkt, F., Eds.; Wiley: Chichester, NY, 2011; Vol. *1*, Chapter 12, pp 511−549.
(69) Cohen, E. R.; Cvitas, T.; Frey, J. G.; Holmström, B.; Kuchitsu, K.; Marquardt, R.; Mills, I.; Pavese, F.; Quack, M.; Stohner, J.; et al. *Quantities, Units and Symbols in Physical Chemistry*, 3rd ed.; IUPAC and Royal Society of Chemistry, RSC Publishing: Cambridge, 2007.
(70) Stohner, J.; Quack, M. In *Handbook of High-Resolution Spectroscopy; Conventions, Symbols, Quantities, Units and Constants for High Resolution Molecular Spectroscopy*; Quack, M., Merkt, F., Eds.; Wiley: Chichester, NY, 2011; Vol. *1*; Chapter 5, pp 263−324.
(71) Ulenikov, O.; Onopenko, G. A.; Tyabaeva, N. E.; Schroderus, J.; Alanko, S. On the Rotational Analysis of the Ground Vibrational State of CH_3D Molecule. *J. Mol. Spectrosc.* **1999**, *193*, 249−259.
(72) Ulenikov, O.; Onopenko, G. A.; Tyabaeva, N. E.; Alanko, S.; Koivusaari, M.; Anttila, R. A New Rotational Study of the Ground Vibrational State of CHD_3. *J. Mol. Spectrosc.* **1997**, *186*, 230−238.
(73) Champion, J. P.; Robiette, A.; Mills, I. M.; Graner, G. Simultaneous Analysis of the ν_1, ν_4, $2\nu_2$, $\nu_2 + \nu_5$ and $2\nu_5$ Infrared Bands of $^{12}CH_3F$. *J. Mol. Spectrosc.* **1982**, *96*, 422−441.
(74) Jensen, P.; Brodersen, S.; Guelachvili, G. Determination of A_0 for $CH_3^{35}Cl$ and $CH_3^{37}Cl$ from the ν_4 Infrared and Raman Bands. *J. Mol. Spectrosc.* **1981**, *88*, 378−393.
(75) Albert, S.; Keppler Albert, K.; Hollenstein, H.; Tanner, C.; Quack, M. In *Handbook of High-Resolution Spectroscopy; Fundamentals of Rotation-Vibration Spectra*; Quack, M., Merkt, F., Eds.; Wiley: Chichester, NY, 2011; Vol. *1*; Chapter 3, pp 117−173.
(76) Quack, M. On the Densities and Numbers of Rovibronic States of a Given Symmetry Species: Rigid and Nonrigid Molecules, Transition States, and Scattering Channels. *J. Chem. Phys.* **1985**, *82*, 3277−3283.
(77) Tarrago, G.; Dupre-Maquaire, J. A New Approach for Vibronic Ground-State Analysis of C_{3v} Molecules: Applications to $^{12}CD_3H$. *J. Mol. Spectrosc.* **1982**, *96*, 170−174.
(78) Ulenikov, O. N.; Bekhtereva, E. S.; Fomchenko, A. L.; Litvinovskaya, A. G.; Leroy, C.; Quack, M. On the 'Expanded Local Mode' Approach Applied to the Methane Molecule: Isotopic Substitutions $CH_3D \leftarrow CH_4$ and $CHD_3 \leftarrow CH_4$. *Mol. Phys.* **2014**, *112*, 2529−2556.
(79) Oldani, M.; Bauder, A.; Loete, M.; Champion, J. P.; Pierre, G.; Hilico, J. C.; Robiette, A. G. Microwave Fourier Transform Spectroscopy of Pure Rotational $\nu_4 - \nu_4$ Transitions and Reanalysis of the ν_2/ν_4 Dyad of Methane-d_4. *J. Mol. Spectrosc.* **1985**, *113*, 229−242.
(80) Drouin, B. J.; Yu, S.; Pearson, J. C.; Müller, H. S. P. High Resolution Spectroscopy of $^{12}CH_3D$ and $^{13}CH_3D$. *J. Quant. Spectrosc. Radiat. Transfer* **2009**, *110*, 2077−2081.
(81) Rothman, L.; Jacquemart, D.; Barbe, A.; Benner, D.; Birk, M.; Brown, L.; Carleer, M.; Chackerian, C., Jr.; Chance, K.; Coudert, L.; et al. The HITRAN 2004 Molecular Spectroscopic Database. *J. Quant. Spectrosc. Rad. Transfer* **2005**, *96*, 139−204.
(82) Watson, J. K. G. Quadratic Herman-Wallis Factors for Symmetric- and Asymmetric-Top Molecules. *J. Mol. Spectrosc.* **1992**, *153*, 211−224.
(83) Graner, G.; Guelachvili, G. Extensive High-Resolution Study of the Crowded Rovibrational CH_3F Spectrum around 3000 cm^{-1}. *J. Mol. Spectrosc.* **1981**, *89*, 19−41.
(84) Bray, C.; Perrin, A.; Jacquemart, D.; Lacome, N. The ν_1, ν_4, and $3\nu_6$ Bands of Methyl Chloride in the 3.4 μm Region: Line Positions and Intensities. *J. Quant. Spectrosc. Radiat. Transfer* **2011**, *112*, 2446−2462.

DOI: 10.1021/acs.jpca.9b02580
J. Phys. Chem. A 2019, 123, 6160−6174